The International Journal of Advanced Manufacturing Technology (2025) 139:5697–5714
https://doi.org/10.1007/s00170-025-16079-5

ORIGINAL ARTICLE

Development of a print head for non-planar additive manufacturing of carbon fiber-reinforced polymers

Johann Kipping[1] · **Thore Kleibrink**[1] · **Thorsten Schüppstuhl**[1]

Received: 24 February 2025 / Accepted: 3 July 2025 / Published online: 6 August 2025

Abstract
In order to realize the potential of high-performance lightweight parts manufactured using the combination of Fused Filament Fabrication (FFF) and Carbon Fiber Reinforced Polymers (CFRP), two main challenges have been identified for a print head design intended for load-oriented non-planar printing. To address these objectives of enabling dynamic layer height variation and fiber cutting, all while avoiding collisions in the printing system, this work presents the methodological development of a new specialized print head. By analyzing the process and taking the existing non-planar printing system into account, the relevant optimization parameters are identified and accurately defined. The methodological development is aligned with the VDI standard 2221 and includes a formal requirement analysis, parameter definition, and functional structure. The solution space is discussed and partial solutions are compared in detail, before the integration and final design are presented. The print head is physically realized, functionally verified by printing CFRP parts, and shown to fulfill all set requirements. Minor necessary changes during the manufacturing and construction of the system are discussed. Finally, the insight, definition, process analysis, and final version are employed to present a further optimized design with a concrete methodological outlook on enabling the load-oriented non-planar FFF of CFRP with this new highly optimized design.

Keywords Print head · Cutting mechanism · Non-planar · Fused filament fabrication · Continuous · Carbon fiber-reinforced composites

1 Introduction

The combination of Carbon Fiber Reinforced Polymers (CFRP) and Additive Manufacturing (AM) shows great potential to unite the advantages of this high performance, lightweight material and flexible, fast manufacturing method [1]. Especially the process variant of Fused Filament Fabrication (FFF) lends itself to this combination. This is mainly due to the possibility of steering individual fiber strands by controlling the nozzle's path, making the most of the composite materials' high degree of anisotropy [2]. While classical planar printing is restricted to in-plane movements, non-planar FFF opens up the possibility of load-oriented printing to all dimensions. Nevertheless, process-specific challenges still remain before this method can deploy its full potential in rapid repair, prototyping, manufacturing in the field, and high-performance applications [3]. Two of the main issues are the required dynamic layer height variation and cutting procedures, while avoiding collisions during the complex positioning and reorientation movements. Further reasoning and derivations of these challenges can be found in [4–6].

To address the issue of collision, a robotic printer for the non-planar AM of CFRP has been developed in prior work [7], which is also displayed in Fig. 1. The machine was methodically designed to produce small-volume CFRP parts using the non-planar FFF process with a high degree of reachability. The printhead fitted to this system was not designed to address the main challenges of layer height variation and cutting. However, the machine was constructed to be able to accommodate such a system in the future [7].

✉ Johann Kipping
johannkipping@tuhh.de

Thore Kleibrink
thore.kleibrink@tuhh.de

Thorsten Schüppstuhl
schueppstuhl@tuhh.de

[1] Institute of Aircraft Production Technology, Hamburg University of Technology, Denickestr. 17, 21073 Hamburg, Hamburg, Germany

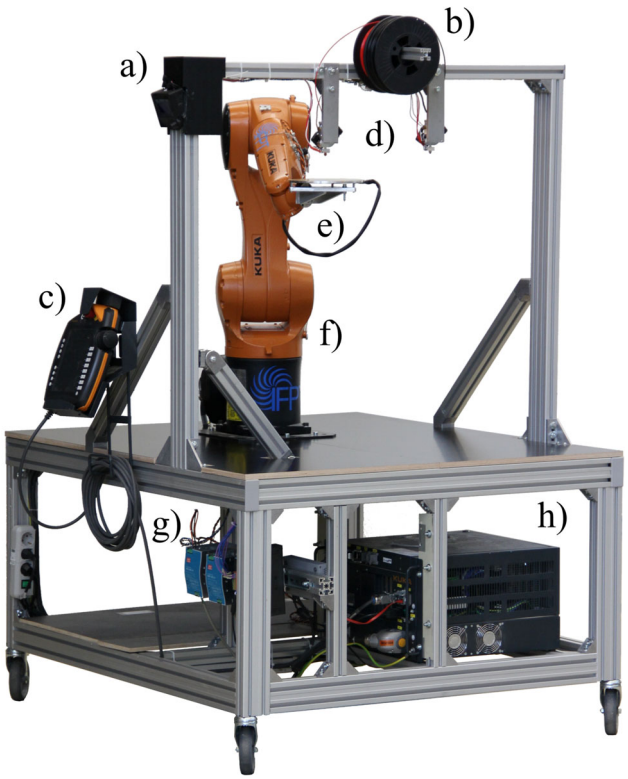

Fig. 1 In prior work developed printing setup without housing taken from [7]. a) Temperature controller, b) material, c) handpanel, d) printheads, e) build plate, f) robot, g) fieldbus, and h) robot controller

1.1 Aim

One of the pivotal challenges for the load-oriented FFF of CFRP parts is the development of a suitable print head. Essential features are dynamic layer height variation, a cutting apparatus with short minimum cutting length, and a maximized clearance angle. This work presents the design, construction, and demonstration of such a system. The development of this system is based on a prior print head that was heuristically designed with the goal of enabling the non-planar FFF of CFRP. The methodical development is documented. Key parameters are comprehensively defined, and the fulfillment of the established requirements is shown.

1.2 Methodology

The developments in this work align with the VDI standard 2221 [8] for the methodical development of technical products and systems. The following main steps are to be followed during development.

1. Clarifying and specifying the task
2. Determining functions and their structures
3. Search for solution principles and their structures
4. Dividing into realizable modules
5. Designing the relevant modules
6. Designing the entire product
7. Elaboration of the implementation and usage specifications
8. Further realization

2 Related research

To identify the deficits of the current state of technology and research, existing publications are reviewed and presented in this section. The contributions of this work are established as well. The section is divided into a part on non-planar printing and the specific challenges and developments of printing CFRP.

2.1 Non-planar printing

In the conventional planar FFF process, a thermoplastic material is melted and deposited along horizontal paths in the form of material beads to form layers [9]. Any three-dimensional structure consists of stacked planar layers with individual geometries. For this reason, the conventional FFF process is often referred to as a 2.5-dimensional manufacturing process, indicating the partial utilization of the third dimension [10]. Non-planar printing, as first described by Chakraborty et al., aims to eliminate this limitation [11].

The objects manufactured by FFF are subject to anisotropic properties in which the bond strength between the individual layers is lower than the tensile strength of the extruded filament strand in the nozzles moving direction [12]. In FFF, the restriction to horizontal movements can lead to the mechanically weaker interfaces being exposed to the load path of the application. A major advantage of non-planar FFF is the ability to align the more resilient orientation with the load direction, which improves the mechanical characteristics of the objects [13]. Alternatively, non-planar printing offers the possibility of reducing the use of support structures by using optimized slicers [14] or even eliminating them altogether by moving the print bed under the print head so that printing always takes place in the direction of the gravitational force [15]. This allows a more resource-efficient manufacturing process to be realized. However, the combination of load-oriented and support-free printing is hard to realize as there exists a trade-off with these two benefits [14]. Eliminating support structures severely limits the possible orientation of the non-planar layers, thus limiting the load orientation capability. Finally, the use of non-planar printing can also be used to improve the surface quality of printed parts [14]. In conventional planar FFF, printed structures suffer from the so-called stair-stepping effect, a deviation from the ideal surface of the

workpiece. The ability to deposit the outermost layer of the part in a single curved layer can reduce this effect significantly. Many state-of-the-art solutions to non-planar slicing use scalar fields to encode a desired property on a tetrahedral mesh, which is then sliced by extracting isosurfaces of this field. The work by Fang et. al. in [16] laid the groundwork for applying this approach to load-oriented non-planar FFF. The vector field of maximum principal directions is used as the basis for computing an optimized vector field. By solving for the scalar field whose gradient approximates the vector field, the load-oriented slices can be obtained as the isosurfaces. This approach was successfully applied to printing CFRP parts in [17]. Another modern approach to non-planar slicing allows to employ planar methods by deforming the mesh before slicing and then applying the inverse transformation to the computed paths. This approach was first introduced in [14] and then successfully applied to CFRP parts by subsequent publications [18].

The use of the non-planar FFF process places new demands on manufacturing machines suitable for its realization. A higher number of degrees of freedom enables the possibility of changing the relative orientation between print bed and print head. As the machine itself limits the possible, collision-free combinations of position and orientation, this machine-specific property is often referred to as reachability [19]. The reachability is essential for slicing and path planning and not trivially computed, making a reachability analysis imperative when planning a non-planar printing system, as carried out in prior work [7]. One of the properties with the highest impact on reachability is the clearance angle of the print head. The definitions used in this work are visually explained on the left of Fig. 2. The prior work [7] also further demonstrates the impact of the clearance angle on the reachability of the print head in the analysis. However, not only the print head and the print bed influence the collision-free operation of the extruder in the working area, but also the material already deposited on the print bed. The slicer is tasked with preventing those collisions with the print heads exclusion zones when planning the print path [20].

Since the idea of non-planar printing was proposed originally, a number of commercial and non-commercial developments have been published that specialized on the implementation of non-planar printing. These will be presented in the following, structured by their highlighting feature.

First, there exist some definitions of the clearance angle in this application, which are explained in this paragraph. In their work, Ahlers et al. define the notions of the "maximum non-planar angle" as well as the "non-planar height" as comparison parameters for print heads used for the non-planar FFF process [20]. These definitions differ from the one used in this work. The differences are highlighted in the visual explanation on the right of Fig. 2. For a macroscopic view, the maximum non-planar angle is equivalent to the tool angle of the print head, while the non-planar height describes a limitation in the height of the non-planar angle. They demonstrate this definition on an Ultimaker 2 print head which has a maximum non-planar angle of 8° and a height of ca. 50 mm. Etienne et al. also define an angle of the nozzle cone and a height that covers the tool from the tip of the nozzle to the start of the carriage [21]. They also define the maximum extent of the printed object and the angle resulting from the height of the tool and the distance of the extent. As the collision angle for their slicer, they use the respectively smaller of the angles they have defined. This definition gives a conservative estimate of the tool angle, especially when it is derived from the tool angle of the nozzle. While it does offer substantial clearance from collisions, it cannot fully utilize the potential of non-planar manufacturing. While these definitions and their respective applications are well suited for comparing planar printing heads in their applicability for non-planar printing, they represent conservative approaches and are of limited use to a generalized application in slicers due to their restriction in height. Mitropoulou et al. show in their work that a compact extruder with a shorter nozzle increases the accuracy of the robot tool center point due to its greater stability in the event of collisions or the application of forces, while the freedom from collisions during printing is greatly reduced [22]. They conclude that an extruder that can better balance these effects of stability and collision freedom can produce more complex geometries. In their work, Shan et al. propose the use of an airbrush nozzle characterized by an extended tip with a more acute angle in order to achieve greater freedom from collision during printing [23].

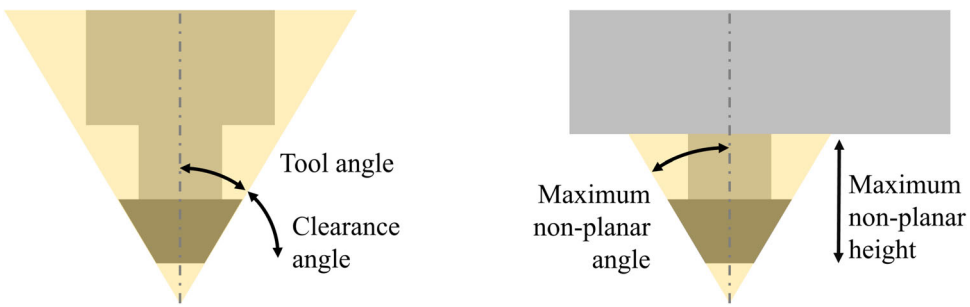

Fig. 2 Visual explanations for the notions of tool angle and clearance angle used in this work on the left and a different definition of similar notions used in prior work [20] on the right

Shortcomings are identified with regard to uniform contact pressure, freedom from collision, and reduction of the support structure. Therefore, they suggest that the nozzle be used exclusively perpendicular to the surface of the part. The company nonplanar.xyz [24] sells nozzles for the FFF process with an extended, thermally insulated shaft to allow greater clearance for non-planar prints. The use of these nozzles with extended heating zones is known to have a negative impact on stringing, oozing, and extrusion control, as they introduce inertia into the control system, which is expected to negatively impact dynamic layer height variation.

2.2 Continuous carbon fiber printing

For the FFF of CFRP, the process variants can be divided into three main categories, when excluding external consolidation, impregnation or curing methods, and separate print heads. These three categories can be seen in Fig. 3.

Towpreg extrusion, as displayed on the left of Fig. 3, gets its name from the material tow, which is a strand of intertwined fibers that are pre-impregnated with a thermoplastic matrix material. As it passes through the hot nozzle, the thermoplastic matrix melts before the pre-impregnated fiber composite filament is applied to the layer [25]. The thermoplastic properties are essential for enabling the FFF process, where the extruded bead fuses with the already deposited material to create a contiguous part. A disadvantage of this method is that a variation in layer thickness is only possible in a very limited range by varying the bead width. This is due to the fixed ratio of matrix material and fiber tow, which makes it unsuitable for addressing the goal of dynamic layer height variation set in this work.

In-situ impregnation, seen in the middle of Fig. 3, uses a hotend with an integrated mixing chamber, in which the bundled dry carbon fibers are impregnated with a molten thermoplastic material just before exiting the nozzle. Kaczmarek et al. found, however, that complete impregnation is almost impossible to achieve using this process [26]. This negatively impacts part quality and mechanical strength, which is the main reason for this process variant being used less frequently today. Additionally, the dry fiber bundle cannot be actively fed into the mixing chamber actively, as the dry fiber does not exhibit sufficient stiffness for feeding. Consequently, a frequently employed method involves pushing them along using the flow of molten matrix material [27]. Since the fiber feed is therefore controlled indirectly via the matrix material feed, the possibilities for modifying the material ratio and thus for varying the layer thickness are concluded to be limited.

A similar hotend to the in-situ impregnation process is used in the coextrusion process, displayed on the right of Fig. 3. In this case, however, the fiber has already been pre-impregnated with a polymer matrix in a previous process step. These can be thermoplastics or thermoplastic-thermoset blends. As a result, the low impregnation performance of in-situ impregnation is eliminated when using this process [28]. As the resulting composite now consists of two matrix materials, the secondary thermoplastic matrix that is added around the towpreg is denoted as co-matrix. Only when using thermoplastic-thermoset blends, active feed of the fiber tow is possible, as the matrix material can be designed to retain enough stiffness inside the hotend, while still being malleable enough to be placed around a bend at the nozzle orifice. These properties make this process variant uniquely suitable for varying layer height dynamically. The possibility to actively feed both co-matrix and towpreg material allows for precise control of the material beads height and width, and thus the final composites composition. A drawback of this method is the limited recyclability due to the inclusion of non-recyclable thermoset components.

Variants of the described processes are briefly described in the following. Towpreg extrusion is very commonly combined with a neat polymer extruder as demonstrated by Markforged [29] to fill gaps with pure matrix or only reinforce parts with the towpreg print head where needed in order to save composite material. The two components are bonded

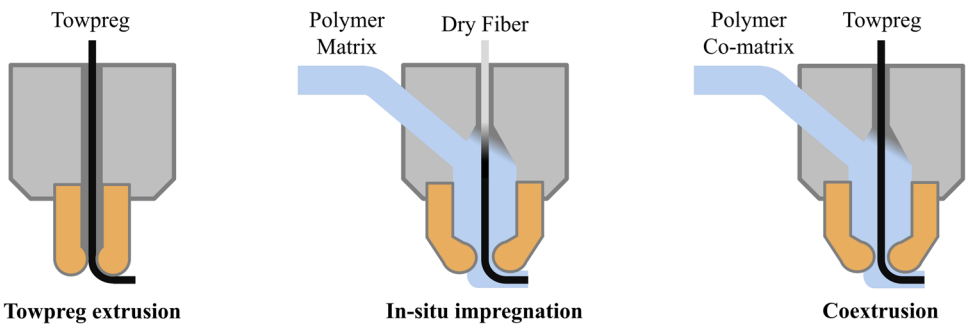

Fig. 3 Extrusion methods for CFRP. With towpreg extrusion, the thermoplastically pre-impregnated filament is directly extruded out of the nozzle; in-situ impregnation denotes the process where dry fiber is impregnated with a thermoplastic matrix inside the print head; coextrusion refers to the mixing of a towpreg impregnated with a thermoplastic or thermoset matrix with a thermoplastic co-matrix

together outside of the nozzle when they are applied to the layer, where the liquefied matrix material is placed over the dispensed fiber [30, 31]. This combination is typically called dual extrusion. With inline impregnation, dry fiber is impregnated before being fed into the printhead, forming the towpreg stock material. In-situ consolidation employs an external pressure compactor to reduce void content and increase part quality. This process can be combined with external energy sources like lasers or other optical heating methods to increase the effectiveness of compaction. In order to use thermosetting materials, these optical energy sources can also be used as a curing method for, e.g., UV-curing resins.

A fundamental property of CFRP is their anisotropic behavior, which manifests itself in a high axial elastic modulus and a comparably lower transversal elastic modulus [32]. To utilize the high tensile strength of Continuous Carbon Fiber (CCF), it is typically recommended to align the fibers according to the local stress state induced by the load case intended for the object. This method is often referred to as fiber steering [33]. Another challenge is the continuity of the CCF. It is not possible to temporarily remove the nozzle from the current manufacturing process to continue printing in a different position or orientation, as is common in the classic FFF process. Slicers that are specialized in the use of continuous fibers by removing the necessity of travel movements inside each individual slice do exist, but those algorithms need to work with loops in order to perform reversing movements [4]. These loops, however, are undesirable as they increase the amount of reorientation points, which can lead to voids and decrease process stability. In order to avoid loops, a cutting unit is required that cuts the fiber in anticipation of the upcoming print progress so that the fiber ends at the desired point in the layer. The smallest possible length of fiber able to be deposited is referred to as the "minimum [cut] length" [34, p. 39]. Shorter cut distances allow smaller geometries to be printed with CFRP, which can increase the fiber volume fraction of the object.

Both non-commercial and commercial developers have been working towards developing functional print heads based on the principles described. Cai and Chen compare different theoretical concepts for the design of print heads specialized in fiber-reinforced polymers in their work [28]. They conclude that the development of a theoretical model to evaluate the thermal coupling effects between the modules of the print head is essential for the development of future print heads. Kuschmitz et al. developed an in-situ impregnating print head for dry carbon as well as dry flax fiber-reinforced polymers designed for planar printing [27]. Their tensile and flexural tests show that the parts they produced exhibited significantly improved strength. However, the achieved process stability was not ideal, and an insufficient fiber-matrix bonding was observed. Kuschmitz et al. propose that further investigation be conducted into the reasons for these inconsistent results and the development of countermeasures. Klimek developed a concept for an extruder with a cutting unit that performs an in-situ impregnation of dry carbon fiber with matrix material [34]. However, this concept was not optimized for non-planar printing. Due to the mixed quality of the CFRP that was achieved, the combined use of the developed filament together with regular filament is recommended. The author was able to show that it is possible to reliably guide carbon fibers through a PTFE tube and drive them via PU-coated rollers. The cutting unit that was developed was promising in theory, but failed because the drive was too weak and could not cut through the weakly bundled fibers. Hribernig picked up Klimek's work on a cutting unit and implemented it in their work on the development of a coextruder print head in which pre-impregnated carbon fibers are bonded with a matrix polymer [35]. As the clearance angle is not the objective of the work, the resulting print head is also not suitable for non-planar printing. A notable feature of the design is the implementation of a reflux valve to eliminate matrix leakage. It is suggested to keep the unguided distance of the fiber as short as possible to prevent any buckling effects. The company Anisoprint offers a range of FFF printers specialized in printing CFRP [36]. Due to the restrictions of the offered printers to three axes, they are limited in their use for non-planar printing. The print head is also not useful for this application, with a different motion system due to the insufficient clearance angle. The brand Markforged also sells FFF printers that specialize in the processing of in-house produced, pre-impregnated CCF [29]. Similar to the model presented by Anisoprint, their model is also not designed for non-planar printing due to the three-axis system and the insufficient clearance angle. In [37], the Mark Two model by Markforged is analyzed, which features a dual extrusion system. In their work, Sauer comes to the conclusion that the model achieves a high level of manufacturing precision with low dimensional deviations, but that the mechanical properties of the printed parts fall short of comparable models and the properties specified by the manufacturer.

3 Development

In this section, the development of the print head is discussed. A full list of requirements, including an analysis of essential target values and definition of the clearance angle and minimum cut length, is presented in the first section. A functional structure is established and followed by setting up the solution space, based on a previous, heuristically developed design. This design was developed by adapting the coextrusion method for use in non-planar printing, but did not include a cutting mechanism and was not methodically developed. It can be seen on the left in Fig. 6. In order to estimate the suitability of partial solutions for cooling, a thermal simulation of

the cold end cooling system is done. Finally, the integration is described.

3.1 Requirements

First, the requirements induced by the non-planar printing process, the printing machine, handling, safety, manufacturing, and maintenance of the print head were identified. A list of the key requirements can be found in Table 1.

0	Global Requirements
0.1	Availability of materials and components
0.2	Tool angle $< 30°$
0.3	Compact design
0.4	20cm $<$ width $<$ 25cm
0.5	Possibility of disassembly & cleaning
1	Controlled local extrusion of melted material
1.1	Co-matrix feed
1.1.1	Steep temperature gradient for hot/cold end separation
1.1.2	Active & precise feeding of the material
1.1.3	Replaceable and cleanable heat break
1.1.4	Manual feeding possible
1.2	CCF feed
1.2.1	Active & precise feeding of the material, while independent and disconnected from mixing chamber
1.2.2	Low leakage of co-matrix material
1.2.3	Manual feeding possible
1.2.4	High positioning accuracy
1.2.5	High accessibility for cleaning
1.3	Cutting unit
1.3.1	Fast ($<$ 2 seconds), precise, damage-free cut
1.3.2	Sufficient cutting force $\geq$ 77N
1.3.3	Defined and constant distance to the nozzle
1.3.4	Cutting length of the carbon fibers $\leq$ 40mm
1.4	Mixing chamber
1.4.1	Short material path between extruder & mixing chamber
1.4.2	Guiding of the CCF material
1.4.3	Positionability & positioning accuracy
1.4.4	Unhindered, straight-line feeding of the CCF material
1.4.5	Heating
1.4.5.1	Heat break for temperature gradient
1.4.5.2	Configurable material temperature [30,..,260]°C
1.4.5.3	Measurement via thermistor
1.4.5.4	Use of a heater cartridge
1.4.7	Mixing the materials immediately before the nozzle outlet
1.5	Extrusion
1.5.1	Anisoprint extrusion nozzle
1.5.2	Dynamically controllable flow rate and co-matrix/towpreg ratio
1.5.3	Prevention of damage to nozzle and composite
1.6	Cooling
1.6.1	Air cooling for part and heatsink
1.6.2	Temperature in heatsink below glass transition temperature of PLA at 59,2°C to prevent clogging
1.6.3	Compact design of mounting solution and cooling fins
1.6.4	Part cooling while respecting the clearance angle
1.6.5	Low cooling effect on nozzle
2	Control system
2.1	Automated printing without user monitoring
3	Movement
3.1	Maximum printing speed for composite 10 mm/s
3.2	Accessibility of all points in the working area
3.3	Height of the freely orientable area 50 mm
3.4	Diameter of the workpiece carrier 200 mm
3.5	Possibility of retraction
4	Safety
4.1	No human interference within the work surface during printing
4.2	No moving parts outside the work surface

Table 1 List of Requirements

3.1.1 Clearance angle

The machine developed in prior work [7] had the goal to guarantee the absence of collisions without the costly and complex computation of inverse kinematics, collision detection, and simulation of the path. To achieve this goal, a precise definition of the clearance angle is crucial to ensure clear reachability conditions for the slicing process.

One of the most immediate influences on clearance angle is the extrusion nozzle. As the fiber has to be bent around the nozzle orifice during printing, a nozzle geometry with a sharp 90° corner at the orifice, which is the case in neat polymer FFF, would lead to immediate fiber breakage during deposition. This is why Anisoprint has developed the nozzle geometry seen in Fig. 4. The rounded corners allow the fiber to be bent continuously and press the composite onto the already deposited material. These rounded corners are marked in green in the Figure. As the optimization of this nozzle geometry is not the focus of this work, this specialized nozzle by Anisoprint is set as fixed, aiding the fulfillment of requirement 0.1 from Table 1.

The clearance angle is typically defined by enveloping the print heads shape with an inverted cone surface, with the central axis of the nozzle being aligned and the smallest possible apex angle. As can be seen in Fig. 4, this definition of a clearance angle leads to very obtuse tool angles. This microscopic perspective is only adequate for collisions regarding the nozzle, which is set as fixed in this work, and limits the possibility of further increasing the clearance angle of the print head. Consequently, the angles definition is split into

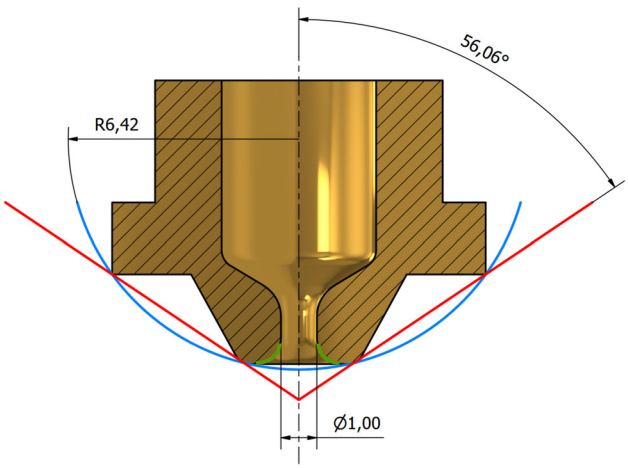

Fig. 4 Microscopic clearance angle, minimum manufacturing radius, and bottleneck diameter of the nozzle. Rounded corners at nozzle orifice marked in green

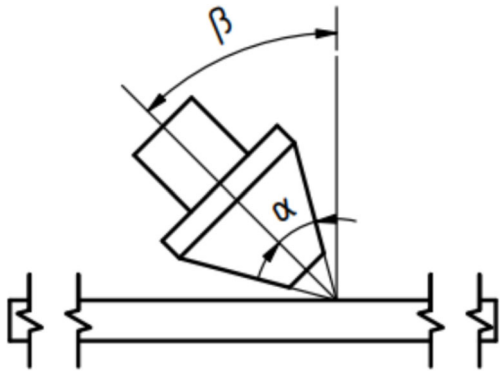

Fig. 5 Macroscopic tool angle α and tilting angle β taken from [7]

micro- and macroscopic viewpoint by the introduction of a quantity described in the following.

The minimum manufacturing radius, represented by the blue circular line in Fig. 4 shows the minimum radius of curved features in a point on a parts constituting layers. As described, it serves as a borderline between the microscopic and macroscopic clearance angle. For objects that are built from slices with a curvature close to the minimum manufacturing radius, the microscopic degree of freedom is decisive while for other objects, the consideration of a macroscopic clearance angle is sufficient.

For objects with curvature above the minimum manufacturing radius, there is no risk of collisions in the microscopic range. A larger clearance angle is defined for them, which lies outside the nozzle. It represents the angle at which collision-free manufacturing is possible in the macroscopic view and is the counter-angle to the tool angle. This can be immediately concluded from the requirements of the nozzle aligning with the surface normal during printing. The tool angle in the macroscopic view is defined by an inverted cone shape touching the widest edge of the nozzle while not being required to have its tip in the working point, as collision around the nozzle tip is prevented through the use of the minimum manufacturing radius. At this point, a connection can also be made with the definitions from [20]. The macroscopic clearance angle can be taken as a continuation of the maximum non-planar angle they used.

To establish a target value for the clearance angle and tool angle, the reachability analysis in section III.A from [7] is consulted. There, the (macroscopic) tool angle is denoted with α and is required to fulfill $\alpha < 45°$, while the tilting angle was set to be $|\beta| \leq 90°$. Both parameters can be seen in Fig. 5 taken from [7]. The tilting angle can be seen to describe the angle between the nozzle axis and the print bed. To improve upon this design and after a qualitative part analysis, the goal for the tool angle is set to $\alpha < 30°$ in this work.

3.1.2 Minimum cut length

The minimum cut length is defined as the distance between the point of fiber cutting and the exit plane from the nozzle. As outlined in Sect. 2, the cut distance should be kept to a minimum in order to allow for the shortest possible distance to be deposited without reversing directions. If reversing movements are allowed, like in [4], this length influences the minimum surface area of a slice that can be filled with fiber, where smaller surfaces can only be constructed using neat polymer. The cutting length depends heavily on the cutting mechanism used, which has a major influence on how close the cutting unit can be placed to the nozzle. A commercially available print head of a planar printer from Anisoprint achieves a minimum cutting length of approximately 40 mm. This serves as a minimum goal for the development in this work, while retaining all the advantages of the non-planar operation.

The two optimization parameters described here can also be seen in Fig. 6, where the previous design of the printhead is shown in a cut cross section on the left and the final redesign described in this work is shown on the right. The previous design was heuristically developed and is inspired by the Anisoprint print head, while enabling non-planar deposition through the introduction of a clearance angle. Balancing the optimization parameters described in this section has been identified to be a major challenge during the design of this print head capable of non-planar FFF of CFRP. This is due to the spacial interrelation of the parameters: when increasing the clearance angle, the available space for the cutting assembly is immediately reduced.

3.2 Functional structure

In the following section, the functions of the device under development are analyzed and structured according to their causal relation. The functionally structure is derived from the process analysis, that can be seen in Fig. 7. In this case, the super-groups *feeding*, *mixing*, *extruding*, and *cooling* are formed.

3.3 Partial solutions

The individual functions and components are assigned to their equivalent industry standard names wherever possible to ensure a standardized development language. Furthermore, partial solutions for the resulting subcomponents will be identified and collected in a morphological box, the results of which can be seen in Table 2, where the solutions that were chosen in the final version are highlighted. The solutions are chosen based on their availability, manufacturing effort, material cost, and compactness, with the focus set on the expected reliability and functionality. The creation of

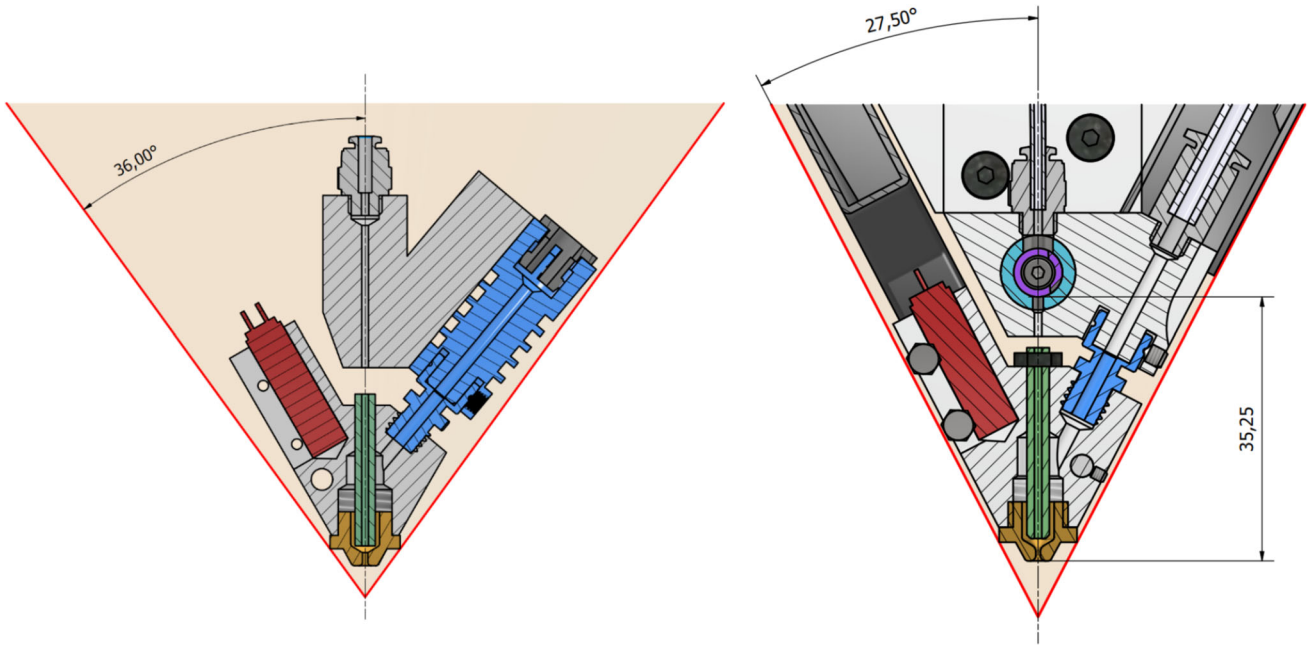

Fig. 6 Cross section of the previous design on the left and redesign described in this work on the right. The two macroscopic optimization parameters of tool angle and minimum cut length are denoted where applicable. Green: fiber tube, blue: heat break, red: heating element, teal: cutting sleeve, purple: cutting blade

multiple overall concept versions is omitted in order to focus more specifically on adding and improving the individual components of the previous version of the printhead. Instead, the approaches found for the individual solutions are compared in detail. The choice for this procedure is motivated by the existence of the previous version that has been shown to be able to print parts without cutting. This practice diverges from the VDI 2221 methodology.

3.3.1 Extrusion method

Even though the previous version of the print head is already designed for the coextrusion process, the reasoning for this choice is given in this section for completeness. Of the methods for extruding CFRP shown in Fig. 3, towpreg extrusion has already been identified as unsuitable, as dynamic layer height variation is impossible due to the fixed ratio of matrix and fiber, which is required for load-oriented deposition. A dual extrusion approach could be employed to construct intermediate layers that consist only of neat polymer. This has the drawbacks of a strongly inhomogeneous fiber distribution and a very limited layer height range in comparison to the coextrusion or in-situ impregnation, as the minimum layer height of the neat polymer extrusion process still has to be taken into account. Additionally, as the number of layers is doubled, the amount of failure points due to weaker interlayer adhesion and the manufacturing time would be approximately doubled as well. Furthermore, the amount of tool changes also increases manufacturing times drastically, while the possible fiber volume fraction would be substantially decreased. In-situ impregnation is disregarded due to its tendency for poor impregnation and thus insufficient mechanical quality, while also exhibiting reduced layer height variability as stated in Sect. 2. Thus, coextrusion remains as the only viable option for high mechanical quality and the ability to dynamically vary layer height.

3.3.2 Co-matrix feed

For feeding the co-matrix filament, there is the option of a single-gear extruder, in which the filament is fed by a driven gear wheel. The necessary contact pressure is created by a tensioned rotating wheel. Another option is to employ a dual-gear extruder, in which two gears rotate in opposite directions to feed the filament. Since the latter method is less prone to slipping and filament grinding, it is chosen in this work.

3.3.3 Pre-impregnated CCF feed

The brand Anisoprint has developed a feeding unit for the pre-impregnated CCF into the guiding tube. The advantages of this system are its proven reliability and availability. Unfortunately, its dimensions are comparatively large. In addition, the motor is positioned in such a way that the unit occupies a large horizontal width when the fiber output is aligned vertically and is therefore not ideally suited for com-

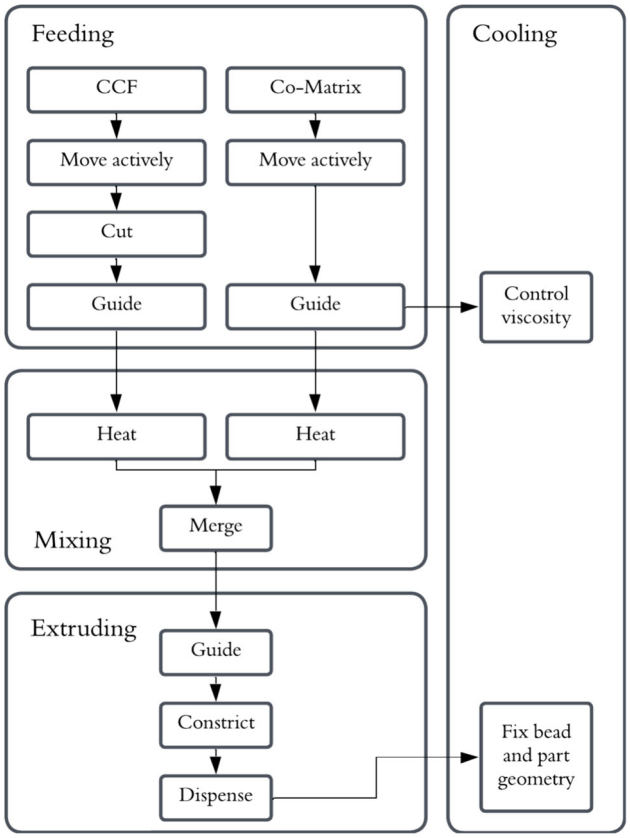

Fig. 7 Functional structure derived from the process analysis. Supergroups are feeding, mixing, extruding, and cooling

pact placement in the clearance angle. In contrast, Sun et al. propose a customized fiber feeding unit [38]. It is space-saving and can therefore be placed in the immediate vicinity of the fiber insert to the cutting unit, which reduces the travel distance of the fiber in the PTFE tube. Since it is not commercially available, it generates additional manufacturing costs that require complicated sourcing of silicone components. Due to the high reliability of the commercial product and the few available field reports on the customized unit, the Anisoprint feeder is chosen.

3.3.4 Cutting unit

The cutting unit and consequently this section is subdivided into the drive and cutting functions.

Pre-impregnated CCF sourced from Anisoprint with a number of 1500 (1.5k) individual carbon fibers is to be used with the printer. From the comparison in [35] of the required cutting force of various impregnated CCF, a required cutting force of less than 0.048 Nm can be estimated. A servo motor that can generate this cutting force and at the same time can be installed in a very space-saving manner is an SG-90 motor with a torque of 0.2541 Nm. As mentioned in Sect. 2, performance problems where noted when using this motor in an axially offset position [34], but since in this case there are no plans to use stronger impregnated CCF and the required cutting force is exceeded by a factor of five, it is foreseeable that this problem will not occur in this application.

Based on the weighted comparisons of cutting principles in [34], a concentric cutting concept is adapted for this work. The Anisoprint brand uses specially developed cutting units with concentric blades in its CFRP-capable planar printers. However, use of this unit is not possible as the horizontal width of the corresponding housing of the units prevents use within a clearance angle above the requirement of 30° while maintaining a minimum cutting length below the requirement of 40 mm. However, it is possible to extract the blade used by Anisoprint and install it in a customized housing that is adapted to the geometric constraints. In this way, a lot of space can be saved in the narrow volume directly behind the heating block, allowing a significant reduction in the minimum cutting distance. Another option is the cutting unit proposed in [35], which would also require the construction of a customized housing. The proposed design is geometrically simple and therefore easy to manufacture. By employing standard sizes, it is possible to modify the design by substituting individual components. However, the design is intended for the use of different fiber diameters and is therefore equipped with two excess feed openings for this application. The author also describes limitations

Table 2 Morphological box where all considered partial solutions are listed. Chosen solutions highlighted

	Solution 1	Solution 2	Solution 3
Co-matrix feed	Dual Gear Extruder	Single Gear Extruder	
Fiber feed	Custom Extruder	Anisoprint Feeder	Fiber feeder [38]
Cutter unit	Anisoprint unit	Anisoprint + combin. unit	Blade and casing [35]
Drive	Belt	Linkage	Gears
Heater cartridge	Standard 6 mm	Industrial product	
Nozzle	nonplanar.xyz	Anisoprint	
Heat break	Custom	Microswiss	Copperhead
Heat sink	Microswiss	Custom heat sink	Custom combination unit
Part cooling	Hinged	Fixed	

in the sourcing of the precision tubes in the required small dimensions and in the desired material pairings. Finally, the dimensions mentioned are in turn too large for the goal of a short minimum cutting length. Consequently, the blade geometry of the Anisoprint cutting unit is selected in conjunction with a customized housing. This variant offers the most effective option for achieving a low minimum cut length and has already been used reliably in the market. Furthermore, the manufacturing of a customized housing offers the possibility of additionally accommodating the function of dissipating thermal energy in the confined space, as elaborated at a later point in Subsection 3.3.6. This unit can be seen in Fig. 6 where the rotating blade is displayed in purple and the stationary sleeve is displayed in teal.

Due to the constrained geometry in the area of the cutting unit, the selected motor cannot be placed coaxially with the rotating concentric blade, but must be moved upward into the less constrained volume. Therefore, some kind of connection is required. One option would be to use a timing belt, which is a compact standard accessory that provides an even load and has a low mass. Because of the rubber material, a belt is resistant to vibrations in the system and tolerates small variations in position. An alternative is stiff links, which are feasible for in-house manufacturing but require precise dimensions. Due to their increased stiffness, these are capable of performing more precise movements under higher load. Yet in this instance, this is not a particularly significant factor, as the speed and torque at the point of contact with the fiber are more crucial for the cutting movements performed than the exact start and end position of the movement. Finally, the torque transmission to the blade shaft could also be realized by multiple gears, which could be advantageous because of the possibility to modify the transmission ratio. On the other hand, a gear structure requires mounting on the assembly plate and takes up a lot of space. As a result, the timing belt is chosen for reasons of flexibility in the event of modifications and its compact constructive form. The low sensitivity to manufacturing inaccuracies is also advantageous when developing a prototype.

3.3.5 Hotend

The hotend denotes all components of the extrusion system whose temperature resides close to the adjustable nozzle temperature during the manufacturing process. In the hotend, thermal energy is transmitted from the heater cartridge, which functions as the heat source, to the heat block, which contains the mixing chamber, and subsequently to the nozzle. The assembly is connected to the remainder of the print head via the heat break, which thermally isolates the remaining structure and prevents the liquefaction of the supplied co-matrix material prior to reaching the heat block. Liquefaction of the co-matrix material prior to its feeding into the heat block is known to result in clogging of the feed channels and a reduction in process stability.

For the heater cartridge, several standard components with a diameter of 6 mm are available for classic FFF printers, as well as smaller industrial components down to about 3.2 mm. However, since there is no shortage of space at the heater cartridge location and standard components are easier to obtain and replace, the standard component is chosen. The heater cartridge is displayed in red in Fig. 6.

The primary function of the heat block is to melt the thermoplastic co-matrix material and heat the pre-impregnated CCF. Prior to this process, the pre-impregnated fiber is fed into the mixing chamber of the heat block via a steel tube with an inner diameter of 1 mm. This fiber tube-based approach, which was inspired by the Anisoprint print head, circumvents the complex manufacturing of a channel with the identical inner diameter in the heat block, thereby reducing the complexity of manufacturing the part. The arrangement of these components is depicted in a cross section seen in Fig. 6, where the previous print head design is depicted on the left and the final redesign on the right. The fiber tube can be seen in green, the heat break in blue, and the nozzle in gold. The co-matrix material is fed into the mixing chamber at an angle through the heat break and a separate channel. In the mixing chamber, the liquid co-matrix material surrounds the fiber tube, which ends just short of the composite nozzle orifice. This fiber tube approach and the small distance between the fiber tube and nozzle orifice are intended to minimize leakage of co-matrix material through the fiber tube and fiber clogging or incorrect fiber feed. The entry of the mixture into the nozzle channel results in the composite material bead.

The heat block is furthermore designed to accommodate a sharp clearance angle. A steep connection bore is chosen in order to enable the placement of the heat sink at a reduced tool angle in comparison to the previous version. This decision is further motivated by the potential focusing of the feed force of the co-matrix material in the direction of the nozzle orifice, as well as an potential increase in process stability due to the reduction of the transverse forces on the section of the fiber situated openly in the mixing chamber when comparing to for example the Anisoprint version. Attention was payed to the sealing surfaces in order to avoid co-matrix leakage. Finally, the thermistor is placed close to the co-matrix inlet and nozzle to avoid a large offset to the actual temperature in the mixing chamber. The heat block can be seen in Fig. 6 as the light gray part that contains the nozzle (gold), fiber tube (green), and heater cartridge (red).

The nozzle was already chosen in Sect. 3.1.1 as the established version sourced from Anisoprint. For an alternative solution, it would be possible to develop a customized extended nozzle similar to the nonplanar.xyz models, which are designed for non-planar FFF processes. As stated earlier,

this is the object of further optimization and not the focus of this work. The nozzle is displayed in Fig. 6 in gold.

For a heat break, the Microswiss M2593 offers compact dimensions and high rigidity. Its thermal conduction is comparatively low due to the titanium material used. However, it also has a complicated connection geometry to the heat sink, which limits modularity. As an alternative, the G2 heat sink of the brand Copperhead is examined. Unlike the Microswiss version, it has a standard heat sink mounting thread. The heat break itself, however, is a complicated structure consisting of three individual parts, which improves the thermal isolation properties but has a negative influence on the stiffness. Stiffness is not a major focus due to the small process forces, but it is desirable in order to ensure the positional accuracy of the nozzle. Moreover, the G2 heat break is comparatively large in relation to other commercial models, which makes it harder to achieve compact dimensions. Finally, due to the weight and possible torque load on the heat break through the entire hotend, the Microswiss heat break is chosen for its higher stiffness properties and smaller dimensions. The heat break can be seen in blue color in Fig. 6.

3.3.6 Cooling

In order to achieve sufficient process stability of the manufacturing process, it is essential to ensure that the thermal energy released is appropriately dissipated from the system. Two areas of the print head mandate active cooling to this end. One of these is the heat sink, which is situated immediately above the heat break and is designed to remove any remaining thermal energy let through the heat break to prevent the co-matrix filament from softening. The other one is the active part cooling of the deposited material immediately after leaving the nozzle.

The small available volume complicates the task of placing a heat sink right after the heat break. A widespread option is the M2597 heat sink from the brand Microswiss. It is an industry-standard part that matches the connection geometry of the discussed heat break of the same brand. It is equipped with horizontal cooling fins, which complicates the supply of cooling air in the smaller tool angle. In addition, its rectangular shape is not optimally adapted to the tool angle. Another option is to develop a single custom part that serves as a dissipation unit for thermal energy. This would allow the use of vertical fins, but would also introduce the risk of unintentional cooling of the hotend if the cooling air is not adequately vented beforehand. A custom solution also allows the heat sink to fit better into the tooling angle and allows a fan to be placed in the clearance angle. A third option considered is to combine the cutter-unit housing with a custom-designed heat sink to form a combination unit. This increases thermal mass to dissipate heat. As with the single version, it allows the use of vertical fins and also allows the placement of a fan in the clearance angle. For this design, the last option of a combined unit is chosen to take advantage of the increased heat distribution. In conventional practice, heat sinks are employed in FFF print heads in conjunction with a fan, with the objective of enhancing heat exchange through the cooling fins by forced convection. It remains to be determined whether the combination unit developed in this work can ensure sufficient process stability or even require this additional cooling. Consequently, a thermal simulation of the combined unit is conducted in Sect. 3.4 using a thermal model as proposed in [28]. The final design of the cooling system is described in Sect. 3.5.

The part cooling system, consisting of a ventilation source and an air duct, would best be placed outside the clearance angle and next to the nozzle. Since this is not possible due to the clearance angle definition, indirect cooling must be used. The GDB4010 model from the brand GDSTIME was selected as the fan unit on the basis of its compactness and availability. Designed as a blower fan, the unit is engineered such that air exits the fan via one of the sides and not the faces. Finally, air ducts should have as little impact on cleaning and repair as possible, so a folding solution based on a rotating axis is chosen over a fixed concept.

3.4 Thermal simulation

In order to assess the performance of the custom-designed heat sink contained in the combination unit with regard to its thermal dissipation properties, a finite element analysis is carried out using the Ansys software [39]. The purpose of this simulation is to gain an estimate on the suitability of the proposed solution and has no further claim to represent an exceptionally adequate or data-driven analysis of the temperature distribution in the system. The simulation includes all components that are significant for heat transfer, including the nozzle, the heat block, the heat break, and the combination unit with the heat sink. To achieve a conservative estimate, further thermal mass, such as that of the mounting plate, is not included. The heat source is defined as a stationary temperature at the contact surface between the heater cartridge and the heat block. For the simulation, this temperature is selected such that the later desired operating temperature of 240°C is present at the thermistor. The model and mesh used can be seen in Fig. 8. The temperature is tested at a constant test point located in the middle of the co-matrix material channel, denoted with TP in Fig. 8. The position of this test point is chosen to lie in the center of the co-matrix channel, as this location is the most relevant in order to avoid process instability due to clogging. The lowest glass transition temperature of the considered co-matrix materials is taken as the threshold value for the maximum permissible temperature. In this case, this is PLA, which has a glass transition temperature of 59.2°C [40]. The simulation is carried

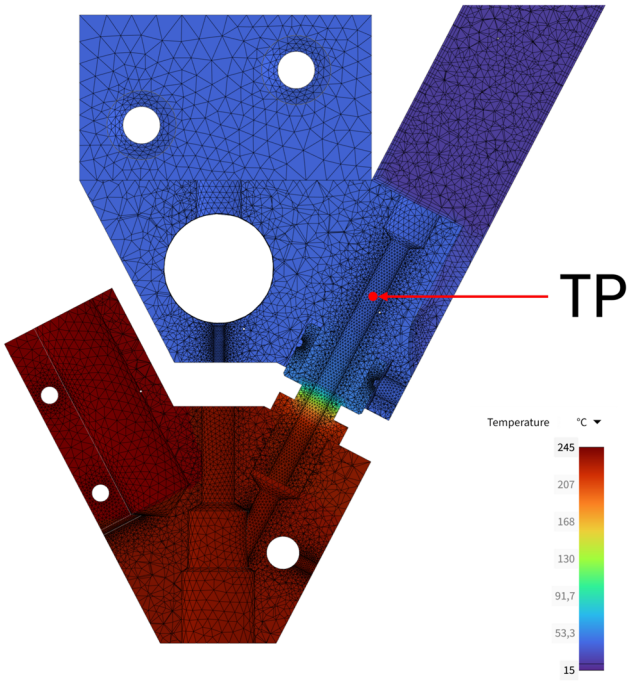

Fig. 8 Thermal simulation with 240°C at the thermistor location and estimated airflow, TP denotes the constant temperature test point. Temperature range indicated by colors

out for various ventilation cases of the heat sink cooling fins, which are described in the following.

The first simulation explicitly excludes any appended air flows. Only heat exchange by radiation on standard parameters is considered. All material parameters are set as standard aluminum, except for the heat break, which was chosen as titanium Ti-6Al-4V with a specific heat capacity of 0.5263 J/g°C and thermal conductivity of 6.7 W/mK. The result of the simulation indicates a temperature of 69.9°C at the test point, which is well above the threshold value. Therefore, it would not be advisable to operate the print head without ventilation.

As outlined in Sect. 3.3.6, most conventional FFF print heads employ a cooling fan to enhance the dissipation of thermal energy. Therefore, a blower cooling fan model GDB4010 from the brand GDSTIME is selected for the heat sink. The outlet of the fan and the inlet of the cooling fins of the heat sink are connected via a customized air duct, which can be additively manufactured. To verify the heat sink with an appended cooling airflow, the convection generated by the fan must first be determined. This is done using the zero pressure flow rate from the data sheet of the implemented blower fan of approximately $1.71\frac{l}{s}$. The software used expects a mass flow as an input value, so it is calculated using the air density assumed to be $1.2041\ \frac{kg}{m^3}$.

$$\dot{m} = \dot{V} \cdot \rho_L = 0.00171\frac{m^3}{s} \cdot 1.2041\frac{kg}{m^3} \approx 2.1\frac{g}{s} \quad (1)$$

As this analysis neglects the flow resistance of the airflow through the ventilation shaft, a conservative safety factor of 10 is applied. This results in a mass flow of $0.21\ \frac{g}{s}$.

The computed airflow is shown with streamlines in Fig. 9. What can be observed is that the rounded bottom vents allow the airflow to be directed away from the heat block, avoiding excessive cooling of the hotend. With the inclusion of this computed airflow, the simulation results in a temperature of 44.5°C at TP, which is the result shown in Fig. 8. This value is distinctly below the threshold and indicates that the printhead in this configuration is suitable for processing the desired co-matrix materials.

A further simulation was carried out to test the effect of an increased cooling surface on the temperature in the co-matrix channel. For this purpose, a version of the combined unit was modeled with a 20 mm longer heat sink and with the connection geometries offset by the same distance. The rest of the combination unit was left in its original state. The simulation with elongated fins results in a temperature of 40.1°C. Although this value undercuts the temperature achieved by

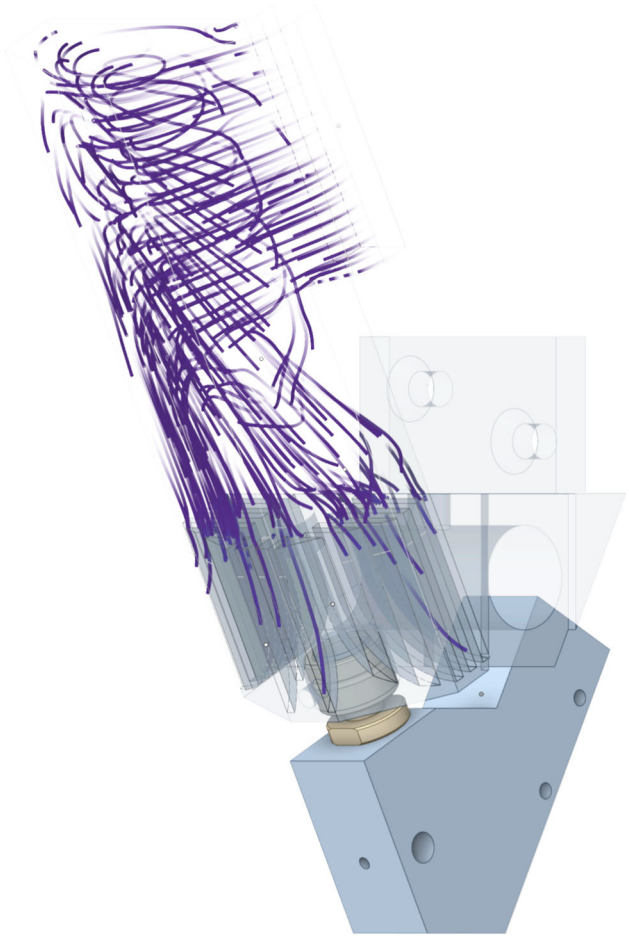

Fig. 9 Visualization of the simulated airflow with streamlines. The rounded bottom vents allow the airflow to flow around the heat block, avoiding excessive cooling of the hotend

the previous concept, the production costs associated with the longer cooling fins are not proportional to the gain achieved through the greater clearance.

All of the partial solutions described in this section have been collected in a morphological box seen in Table 2, where the chosen solutions are highlighted.

3.5 Integration

For the integration into the final concept, emphasis is set on parameters whose influence extends beyond individual modules and on functions that link individual modules together. These include geometric dependencies and effects on the clearance angle due to the serial installation of components. The installation chain starts with the nozzle and ends with the combination unit that is ultimately connected to the assembly panel. Additionally, special attention is paid to the direct accessibility of subcomponents for disassembly and cleaning, as well as to the compactness of the structure and the accuracy of filament and fiber guidance. Since this development is intended as a prototype, several options have been implemented for subsequent adjustment or modification. These include screw connections as the main connection method and the use of standard threads. In order to enable quick access to the filament guide, a lift-off extruder design that allows the extruder components to be moved upwards through the use of slotted holes is implemented. A two-part ventilation shaft connected by a snap-fit joint is also adapted for this purpose. Tensioning of the timing belt is provided by an adjustable tensioner pulley, which was deemed unnecessary and removed during the actual assembly, as described in Sect. 4.2. Finally, a mounting option has been implemented to the T-slot structural frame of the robotic printer. All the components, their method of integration, and the overall design can be found in Fig. 10 seen from the front and in Fig. 11 seen from the back. The components are labeled and their names can be found in the figures' captions.

4 Results

This section contains the presentation and analysis of the resulting final design of the print head as well as its physical realization and functional verification. The achieved optimization parameter values discussed in the next section are followed by details on the manufacturing and construction of the final version. Finally, the printhead is shown to fulfill all set requirements and be able to additively manufacture CFRP parts.

4.1 Clearance angle and cutting distance

In the resulting structure, the tool angle is 27.5°. Being the counter-angle to the tool angle, the clearance angle therefore

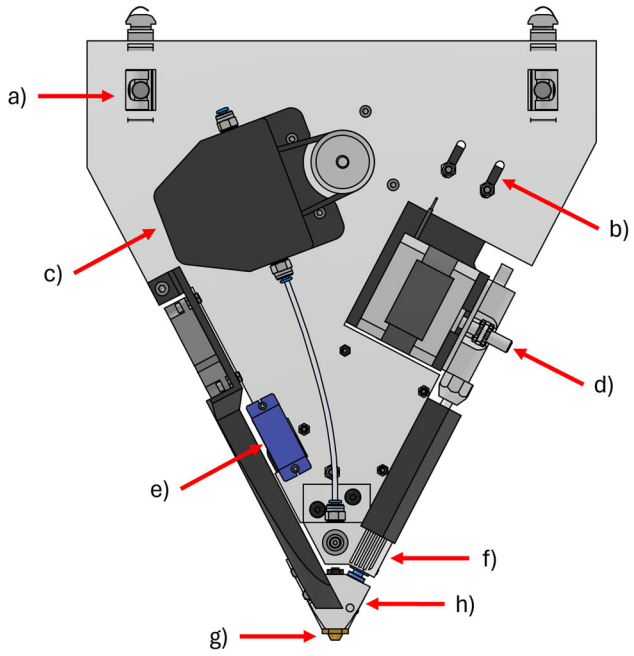

Fig. 10 Front view of the print head design: a) assembly panel, b) lift-off guide, c) CCF feeder unit, d) co-matrix filament extruder, e) cutting-unit servo motor, f) cutting-unit/heat sink combination unit, g) nozzle, and h) heat block

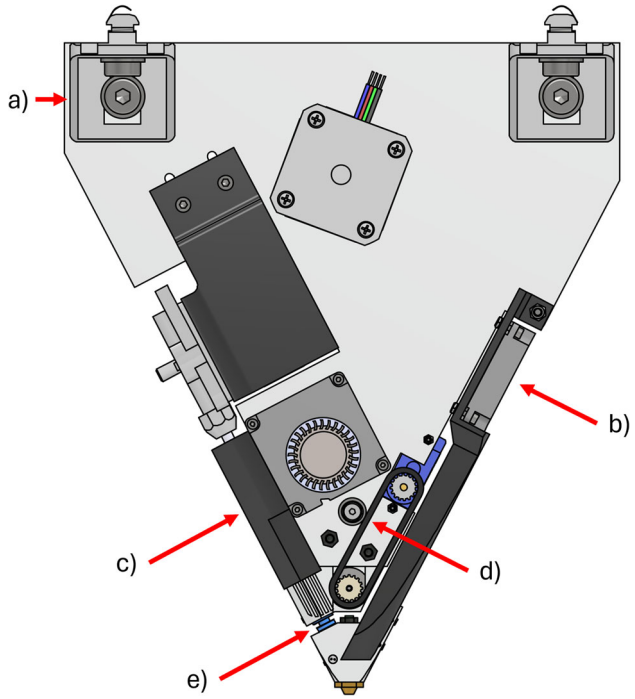

Fig. 11 Back view of the print head design: a) angle bracket, b) part cooling, c) heat sink cooling, d) cutting-unit drive belt with tensioner pulley, and e) heat break

results in $90° - 27.5° = 62.5°$. This result undercuts the requirement set by 2.5.

A promising cutting unit has been successfully added to the design. The resulting minimum cutting distance is 35.25 mm. In practice, the thickness of the slicer-configured layer at the current point in the objects printing path, as well as the accuracy of the depositing process, also have a marginal additive influence on the actual minimum cut length. The distance achieved is significantly less than that of the commercially available model, despite the fact that the commercial model is only suitable for planar printing.

These two optimization parameters can be seen in the final version of the printhead on the right of Fig. 6.

4.2 Physical realization

The print head described in this paper has been physically realized, as can be seen in Fig. 12. Up to minor modifications to the planned version, the design could be implemented as planned. These modifications and more details on manufacturing and construction are provided in the following.

The combination unit and mixing chamber were milled from aluminum, while the backing plate was cut from steel. Due to this combination, corrosion should be monitored but is not expected to cause severe issues. The material choices are motivated by the fact that the print head is stationary in the configuration used in this setup, which allows for materials with high stiffness and density. Manufacturing is this positively impacted by the high stiffness and not negatively impacted by the high mass. The cutting unit was inserted into the bore with its orientation set to have its cutting surfaces on the bottom exit of the combination unit. The tightening roller was removed, and size-adapted pulleys were printed to ensure a tight belt. The position of the servo had to be adjusted to enable the use of an available standard-sized belt. Additionally, the cutout for the co-matrix feeding motor had to be increased to enable the use of an available motor. As an insufficient temperature control authority was observed during initial heating tests, the position of the thermistor was switched to the other side of the mixing chamber, which was able to eliminate the problem. Further investigations, combined with a more sophisticated thermal simulation, should be done to optimize the temperature management and control to ensure consistent and exact temperatures at the nozzle and mixing chamber. No other modifications were necessary during the construction of the print head.

The printing system is controlled by 5-axis GCode that is read by the Kuka.CNC package. The package uses a CNC-kernel for controlling the robots movement. For every movement command in the code, the current layer height is set as a parameter. This parameter is monitored by the Kuka.RSI package, which controls the extruder motors in accordance with the currently set layer height. The velocity target values for the motors are sent to a stepper motor driver that is directly connected to the robot controller over EtherCAT. To control the servo used in the cutting unit, a toggle signal is switched in the GCode and sent through the digital outputs of the robot controller by use of the Kuka.RSI package. This signal is then read by an Arduino MEGA and translated into a PWM signal for the servo and cutting unit. A more elegant solution would be the addition of a PWM-enabled module on the field bus, which would eliminate the need for the Arduino.

4.3 Functional verification and fulfillment of requirements

This section aims to verify the functionality of the printhead with respect to the functional analysis and the list of requirements. The groups and structure described in Sect. 3.2 and displayed in Fig. 7 have been successfully implemented, as demonstrated by printing the parts seen in Fig. 12. No leakage

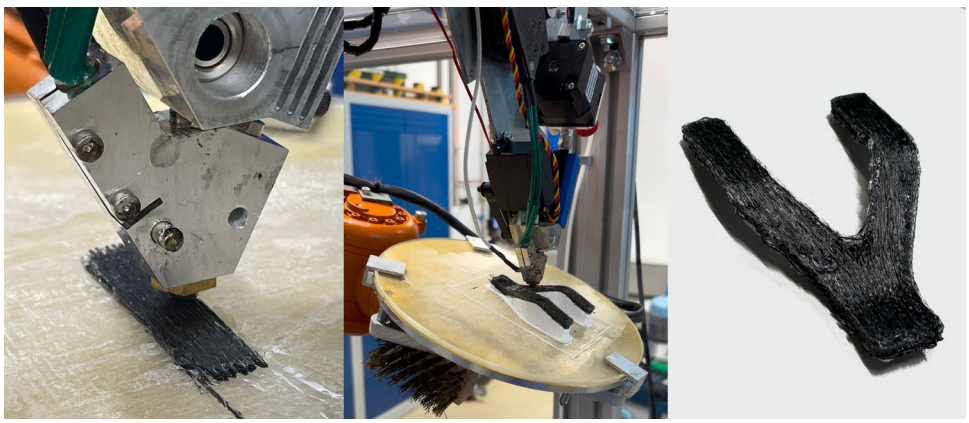

Fig. 12 Physical realization of the printhead during functional verification; part cooling vent and fan flipped up for better visibility. Left: printed coupon shows cuts, middle: non-planar printing with dynamic layer height variation, right: final printed part

could be observed during printing, and the necessary time for a single cut does not exceed 2 s with a clean cutting result.

Going through the list of key requirements in Sect. 3.1, it can be concluded that all key requirements have been fulfilled by the final print head design and physical realization. As was already stated, temperature stability could be improved. The capability of dynamic layer height variation has been investigated and confirmed in detail in an extensive study, which will be part of a future publication. The negative impact on temperature stability of the part and cold end cooling solutions was investigated by temporarily switching the fans off. No negative effects of the cooling solutions could be observed.

5 Conclusion

In this work, a print head for the non-planar load-oriented FFF of CFRP is methodically developed and functionally verified. For this purpose, the procedure of VDI 2221 is used as a guideline. Requirements are formulated, and the optimization of the clearance angle and the shortest possible cutting length are defined as objectives of the work. Furthermore, unambiguous definitions are found for the established optimization parameters. Subsequently, a functional structure is established, with the help of which partial solutions for subcomponents are created and collected in a morphological box. Deviating from VDI 2221, the variants are not compared for overall solutions but for the respective individual solutions. The central component of the concept is a combination unit in which a cutting unit and a heat sink for dissipating thermal energy are combined. To verify the functionality of the overall structure, the solution found is modeled using a computer-aided design program, and the viability of the cooling solution is confirmed using a thermal simulation. This shows that the designed combination unit is only able to keep the temperature in the feed channel of the co-matrix material below the required limit value with the aid of the fan. The thermal model is also used to investigate the use of larger cooling surfaces. However, this option is identified as unnecessary for a functioning print head. The individual solutions found are integrated into an overall concept that surpasses the goals set for the optimization parameters. The result of this study is a design that implements the desired cutting unit and comfortably undercuts the requirements on the two optimization parameters of clearance angle and minimum cutting length. Finally, the construction and testing of the physical realization is discussed, with the necessary minor changes to the design being reported. Printing the test parts served as functional verification and confirmation that all requirements set during the development phase are met by the final print head. The success of this verification implies the conclusion that the main challenges of non-planar CFRP FFF can be addressed with this printhead design, namely dynamic layer thickness variation and cutting while avoiding collisions, as stated in the introduction.

6 Outlook

The printhead designed in this publication was able to address the major challenges stated in the introduction, while a major difficulty was noted in balancing the optimization parameters of cutting length and clearance angle.

When taking the next logical step of analyzing the geometrical range and curvature profiles of slices that can be manufactured with the final version of the printhead, one major limitation of the current version can be discovered. This results from the consideration of the printhead colliding with already deposited material and the infinite extension of the clearance angle defined by the inverted cone. When taking concave features into account, the tool angle impacts the maximum curvature of such features severely. Especially for deeper concave features, this becomes problematic as the inverted cone cannot reach arbitrarily deep into a cavity.

The tilting angle β from [7] is $|\beta| \leq 90°$, which can not be achieved for a nonzero clearance angle. From this reasoning, it can be concluded that, for collisions with already deposited material, not only the tool angle, but also the clearance around the nozzle cone is important. To measure this clearance, a new measure can be introduced called the tool-cone height, which can be seen in Fig. 13. The figure shows an idea for an improved design, featuring an acute needle-tip printhead. The major modification to enable this redesign was the reorientation of the co-matrix feed, which is not expected to impact the functionality of the print head, as the Anisoprint print head features an even sharper bend of 90°. Flow simulations should be done, however, to verify this claim.

An additional modification seen in Fig. 13 is a custom nozzle design that further reduces the wasted space inside the mixing chamber with a more compact and streamlined design. This redesign eliminates the need for a separation of microscopic and macroscopic clearance angles, as both align perfectly at their boundaries. An immediate conclusion for future work from this redesign would be the thorough analysis of the resulting system. This should include a more sophisticated thermal simulation with a practical validation to first increase control authority and temperature stability by optimizing the thermistor position and heater cartridge size, but also to model the interfacing surface to the liquid co-matrix in the mixing chamber. This could be used in conjunction with a material analysis of the co-matrix for a flow simulation to identify the expected back pressure on the co-matrix feed and the gain insight into the flow profile and temperature stability inside the mixing chamber. Finally, the nozzle orifice shape and cross section, which have a great impact on the process stability and compaction effect, could

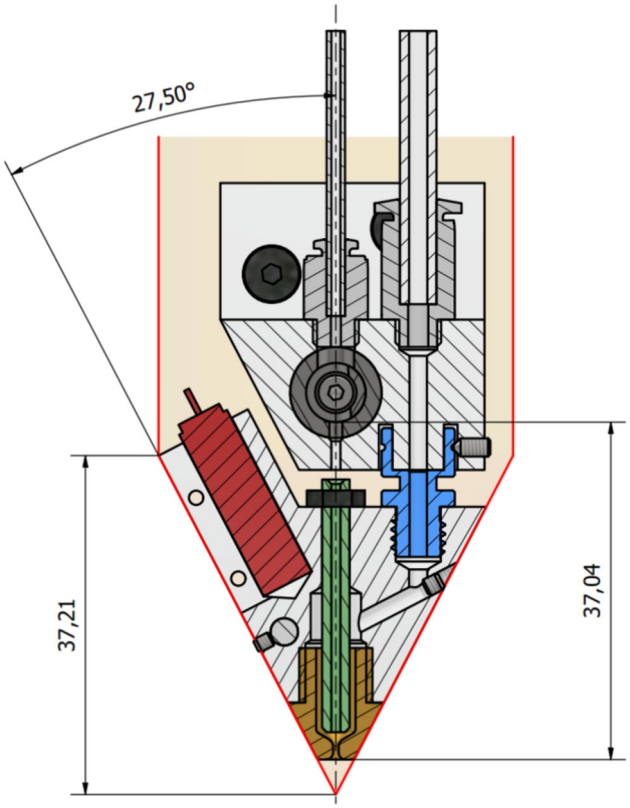

Fig. 13 Version of the proposed printhead with optimized nozzle cross section, compact design, and introduction of the additional parameter tool-cone height. This redesign would enable the manufacture of deeper concave features in part and slice geometry

be optimized using the information gained on by the flow simulation.

Finally, these insights would make the development of an optimized needle-tip printhead regarding the following topics possible

- Temperature distribution and stability
- Component size, position, and shape
- The three optimization parameters of clearance angle, minimum cut length, and tool-cone height
- Nozzle orifice and cross-section geometry.

Addressing these points would severely impact the spectrum of manufacturable parts, especially regarding concave geometries and process stability.

Author contribution CRediT authorship contribution statement: **Johann Kipping:** Conceptualization, methodology, formal analysis, investigation, resources, writing—review and editing, visualization; **Thore Kleibrink:** formal analysis, investigation, original draft preparation, methodology; **Thorsten Schüppstuhl:** writing—review and editing, funding acquisition, supervision, project administration; All authors have read and agreed to the published version of the manuscript.

Funding Open Access funding enabled and organized by Projekt DEAL. This work was supported by the Deutsche Forschungsgemeinschaft (DFG, German Research Foundation) — Grant number 550194375

Data and code availability All data and models generated or used during the study appear in the submitted manuscript.

Materials availability All Materials used in this work can be sourced.

Code availability Not applicable

Declarations

Ethics approval and consent to participate Not applicable

Conflict of interest The authors declare no competing interests.

References

1. Liu T, Zhang T, Chen Y, Wang W, Jiang Y, Huang Y, Wang CCL (2025) Neural co-optimization of structural topology, manufacturable layers, and path orientations for fiber-reinforced composites. arXiv:2505.03779
2. Li N, Link G, Wang T, Ramopoulos V, Neumaier D, Hofele J, Walter M, Jelonnek J (2020) Path-designed 3d printing for topological optimized continuous carbon fibre reinforced composite structures. Composites Part B: Eng 182:107612. https://doi.org/10.1016/j.compositesb.2019.107612
3. Zhang Y, Zheng W, Wang Y, Ma K, Feng X, Ji Q, Guo W, Lu B (2025) A review of 3d printing continuous carbon fiber reinforced thermoplastic polymers: materials, processes, performance enhancement, and failure analysis. Polymer Composites. https://doi.org/10.1002/pc.29895
4. Kipping J, Nettig D, Schüppstuhl T (2024) Looping: load-oriented optimized paths in non-planar geometry. Additive Manufact 94. https://doi.org/10.1016/j.addma.2024.104426
5. Kállai Z, Kipping J, Schüppstuhl T (2024) Closing the gap: exploring approaches for printing lightweight curved pipes with carbon fiber reinforced thermoplastics. The European Society for Composite Materials (ESCM) and the Ecole Centrale de Nantes. https://doi.org/10.15480/882.13713. https://hdl.handle.net/11420/52078
6. Steltner K, Kipping J, Schüppstuhl T, Kriegesmann B (2025) A workflow for designing stiffness-optimized structures in the context of additive manufacturing of endless fiber-reinforced composites. J Thermoplastic Composite Mater. https://doi.org/10.1177/08927057251332788

7. Kipping J, Nettig D, Kallai Z, Schueppstuhl T (2023) A robotic printer for nonplanar additive manufacturing of carbon fiber reinforced polymers. ISR Europe 2023; 56th International Symposium on Robotics. https://ieeexplore.ieee.org/abstract/document/10363073
8. Projektmanagement P (2019) VDI 2221 Blatt 1 - Entwicklung technischer Produkte und Systeme - Modell der Produktentwicklung. Produkt- und Prozessgestaltung. https://www.vdi.de/richtlinien/details/vdi-2221-blatt-1-entwicklung-technischer-produkte-und-systeme-modell-der-produktentwicklung
9. Bikas H, Stavropoulos P, Chryssolouris G (2016) Additive manufacturing methods and modelling approaches: a critical review. Int J Advanced Manufact Technol 83(1–4):389–405. https://doi.org/10.1007/s00170-015-7576-2
10. Pelzer L, Hopmann C (2021) Additive manufacturing of non-planar layers with variable layer height. Additive Manufact 37:101697. https://doi.org/10.1016/j.addma.2020.101697
11. Chakraborty D, Aneesh Reddy B, Roy Choudhury A (2008) Extruder path generation for curved layer fused deposition modeling. Computer-Aided Design 40(2):235–243. https://doi.org/10.1016/j.cad.2007.10.014
12. Gao X, Qi S, Kuang X, Su Y, Li J, Wang D (2021) Fused filament fabrication of polymer materials: a review of interlayer bond. Additive Manufact 37. https://doi.org/10.1016/j.addma.2020.101658
13. Singamneni S, Roychoudhury A, Diegel O, Huang B (2012) Modeling and evaluation of curved layer fused deposition. J Mater Process Technol 212(1):27–35. https://doi.org/10.1016/j.jmatprotec.2011.08.001
14. Zhang T, Fang G, Huang Y, Dutta N, Lefebvre S, Kilic ZM, Wang CCL (2022) S3-slicer: a general slicing framework for multi-axis 3D printing. ACM Trans Graphics 41(6):1–15. https://doi.org/10.1145/3550454.3555516
15. Dai C, Wang CCL, Wu C, Lefebvre S, Fang G, Liu Y-J (2018) Support-free volume printing by multi-axis motion. ACM Trans Graphics 37(4):1–14. https://doi.org/10.1145/3197517.3201342
16. Fang G, Zhang T, Zhong S, Chen X, Zhong Z, Wang CCL (2020) Reinforced FDM: multi-axis filament alignment with controlled anisotropic strength. ACM Trans Graph 39(6). https://doi.org/10.1145/3414685.3417834
17. Fang G, Zhang T, Huang Y, Zhang Z, Masania K, Wang CCL (2024) Exceptional mechanical performance by spatial printing with continuous fiber: curved slicing, toolpath generation and physical verification. Additive Manufact. 82. https://doi.org/10.1016/j.addma.2024.104048
18. Zhang T, Liu T, Dutta N, Chen Y, Su R, Zhang Z, Wang W, Wang CCL (2025) Toolpath generation for high density spatial fiber printing guided by principal stresses. Composites Part B: Eng 295:112154. https://doi.org/10.1016/j.compositesb.2025.112154
19. Wu C, Dai C, Fang G, Liu Y-J, Wang CCL, (2017) RoboFDM: a robotic system for support-free fabrication using FDM. In, (2017) IEEE international conference on robotics and automation (ICRA), pp 1175–1180. IEEE, Singapore, Singapore. https://doi.org/10.1109/ICRA.2017.7989140. http://ieeexplore.ieee.org/document/7989140/
20. Ahlers D, Wasserfall F, Hendrich N, Zhang J (2019) 3d printing of nonplanar layers for smooth surface generation. In: 2019 IEEE 15th International conference on automation science and engineering (CASE), pp 1737–1743. https://doi.org/10.1109/COASE.2019.8843116
21. Etienne J, Ray N, Panozzo D, Hornus S, Wang CCL, Martínez J, McMains S, Alexa M, Wyvill B, Lefebvre S (2019) CurviSlicer: slightly curved slicing for 3-axis printers. ACM Trans Graph 38(4):1–11. https://doi.org/10.1145/3306346.3323022
22. Mitropoulou I, Bernhard M, Dillenburger B (2020) Print paths keyframing: design for non-planar layered robotic FDM printing. In: Symposium on Computational Fabrication, pp 1–10. ACM, Virtual Event USA. https://doi.org/10.1145/3424630.3425408. https://dl.acm.org/doi/10.1145/3424630.3425408
23. Shan Y, Shui Y, Hua J, Mao H (2023) Additive manufacturing of non-planar layers using isothermal surface slicing. J Manufact Processes 86:326–335. https://doi.org/10.1016/j.jmapro.2022.12.054
24. nonplanar.xyz: non-planar | nonplanar.xyz. Accessed: 2025-01-02. https://www.nonplanar.xyz/
25. Wang F, Wang G, Wang H, Fu R, Lei Y, He J (2023) 3D printing technology for short-continuous carbon fiber synchronous reinforced thermoplastic composites: a comparison between Towpreg extrusion and in situ impregnation processes. Chinese J Mech Eng.: Additive Manufact Front 2(3):100092. https://doi.org/10.1016/j.cjmeam.2023.100092
26. Kaczmarek D, Walczyk D, Garofalo J, Sobkowicz-Kline M (2021) An investigation of in situ impregnation for additive manufacturing of thermoplastic composites. J Manufact Processes 64:972–981. https://doi.org/10.1016/j.jmapro.2021.02.018
27. Kuschmitz S, Schirp A, Busse J, Watschke H, Schirp C, Vietor T (2021) Development and processing of continuous flax and carbon fiber-reinforced thermoplastic composites by a modified material extrusion process. Materials 14(9). https://doi.org/10.3390/ma14092332
28. Cai H, Chen Y (2024) A review of print heads for fused filament fabrication of continuous carbon fiber-reinforced composites. Micromachines. 15(4):432. https://doi.org/10.3390/mi15040432. Number: 4 Publisher: Multidisciplinary Digital Publishing Institute
29. Markforged: industrial additive manufacturing platform | Markforged. Accessed: 2025-01-02. https://markforged.com/?__geom=%E2%9C%AA
30. Ochana I (2024) Comparative accuracy analysis of continuous fiber composite printers: coextrusion vs. dual-nozzle technology. Materials Research Forum LLC., Millersville PA, USA. Pages: 136. https://doi.org/10.21741/9781644903131-14
31. Kabir SMF, Mathur K, Seyam A-FM (2020) A critical review on 3D printed continuous fiber-reinforced composites: history, mechanism, materials and properties. Composite Struct 232. https://doi.org/10.1016/j.compstruct.2019.111476
32. Shirasu K, NAGAI C, Naito K, (2020) Mechanical anisotropy of PAN-based and pitch-based carbon fibers. Mech Eng J 7. https://doi.org/10.1299/mej.19-00599
33. Smith R, Qureshi Z, Scaife R (2016) El-Dessouky H (2016) Limitations of processing carbon fibre reinforced plastic/polymer material using automated fibre placement technology. J Reinforced Plastics Composites 35(21):1527–1542. https://doi.org/10.1177/0731684416659544
34. Klimek P-C (2020) Entwicklung eines Extruders mit Schneidemechanismus für die FFF-Generative Fertigung eines Kunststoff-Endlosfaser-Komposits. Electronic Theses and Dissertations. http://epub.technikum-wien.at/obvftwhsmmig/9750846
35. Hribernig T (2021) Extruder with cutting mechanism for continuous fiber-reinforced fused filament fabrication using impregnated fibers. Electronic Theses and Dissertations. http://epub.technikum-wien.at/obvftwhsmmig/9749428
36. Anisoprint: continuous fiber 3D printing for manufacturing of optimal composites. Accessed: 2025-01-02. https://anisoprint.com/
37. Sauer MJ (2018) Evaluation of the mechanical properties of 3D printed carbon fiber composites. Electronic Theses and Dissertations. https://openprairie.sdstate.edu/etd/2436
38. Sun W, Feinberg A, Webster-Wood V (2022) Continuous fiber extruder for desktop 3D printers toward long fiber embedded hydrogel 3D printing. HardwareX 11:00297. https://doi.org/10.1016/j.ohx.2022.e00297
39. Inc A (2025) Ansys | Engineering Simulation Software — ansys.com. Accessed: 2025-01-03. https://www.ansys.com/

40. Żenkiewicz M, Richert J, Rytlewski P, Moraczewski K, Stepczyńska M, Karasiewicz T (2009) Characterisation of multi-extruded poly(lactic acid). Polymer Testing 28(4):412–418. https://doi.org/10.1016/j.polymertesting.2009.01.012